Heavy-Fermion Behavior and Electrochemistry of $Li_{1.27}Mn_{1.73}O_4$

M. Kopeć, J. R. Dygas, F. Krok, A. Mauger,* F. Gendron, B. Jaszczak-Figiel, A. Gagor, K. Zaghib, and C. M. Julien

Institut des Nanosciences de Paris, UMR 7588, and Institut de Minéralogie et Physique de la Matière Condensée, UMR 7590, Université Pierre et Marie Curie-Paris 6, 140 rue de Lourmel, 75015 Paris, France, Faculty of Physics, Warsaw University of Technology, Koszykowa 75, 00-662 Warszawa, Poland, Faculty of Chemistry, Warsaw University of Technology, Noakowskiego 3, 00-664 Warszawa, Poland, Institute of Low Temperature and Structure Research, Polish Academy of Sciences, Okólna 2, 50-950 Wrocław, Poland, and Institut de Recherche d'Hydro-Québec, 1800 Boulevarde Lionel Boulet, Varennes, Quebec, Canada J3X 1S1

Received March 3, 2009. Revised Manuscript Received April 15, 2009

The spinel of nominal composition $Li_4Mn_5O_{12}$ has been prepared by the wet chemistry technique and characterized by structural analysis (X-ray diffractometry, Raman spectroscopy), magnetic properties including electron spin resonance (ESR), and thermal properties (specific heat). Both structural and magnetic analyses reveal that the physical and electrochemical properties are importantly influenced by the presence of Li_2MnO_3 impurity phase. The presence of this additional phase reduces the average oxidation state of manganese according to a disproportionation reaction so that the final composition of the spinel phase is $Li_{3.8}Mn_{5.2}O_{12}$ (or $Li_{1.27}Mn_{1.73}O_4$). Because of the important geometric frustration of the magnetic interactions and dilution of the antiferromagnetic interactions, no magnetic ordering is observed in the temperature range investigated. The anomalous magnetic properties, including the Dysonian profile of the ESR line, show that the material is metallic. The Sommerfeld constant is 308 mJ/(K^2) per mole of $Li_{1.27}Mn_{1.73}O_4$, which shows that this material belongs to the class of heavy-fermion systems like LiV_2O_4 or $LiTi_2O_4$. These heavy fermions are the minority-spin $t_g\downarrow$ electrons of Mn^{3+} ions that have an reduced effective masse $m/m_0 = 467$. The electrochemical properties show that the specific capacity of $Li_{3.8}Mn_{5.2}O_{12}$ at charge rate 1C is 163 mA h/g, a large value that is possibility due to the to insert Li up to the composition $Li_{6.8}Mn_{5.2}O_{12}$. The origin of the disproportionation, and the flat voltage in the lithiation process, are discussed in the framework of the stability of the Mott insulator phase with respect to the metallic phase.

1. Introduction

The lithium manganese spinel is the subject of intensive investigations, because this material is promising for use as positive electrode for advanced lithium-ion batteries.[1,2] In spinel notation, the stoichiometric compound is represented by the formula $(Li)_{8a}[Mn_2]_{16d}O_4$. The oxygen ions form a cubic-close-packed array occupying 32*e* sites of the space group *Fd3m.* The atomic arrangement is illustrated in Figure 1. Half of the Mn ions are in the Mn^{4+} configuration, and half of them in the Mn^{3+} configuration. As a result, it is difficult to prepare samples of good quality, because the Jahn−Teller Mn^{3+} ions favor lattice distortions. Indeed, when Li is inserted to form $Li_{1+x}Mn_2O_4$, a cooperative Jahn−Teller distortion reduces the crystal symmetry from cubic-spinel to tetragonal,[1] so that the electrode must be protected against overdischarge. Even so, the local lattice distortion upon changing the valence of Mn limits the number of cycles that this cathode element can suffer, and the electrode is fragile and can dissolve. To avoid this effect and increase the structural stability, the amount of Mn^{3+} ions must be reduced (average valence larger than 3.5). This can be done by modification of the composition of the spinel electrode,[3] in particular by substitution of lithium for manganese on the octahedral 16*d* sites, forming the solid solution $(Li)[Li_yMn_{2-y}]O_4$ (or $Li_{1+y}Mn_{2-y}O_4$). Upon increas-

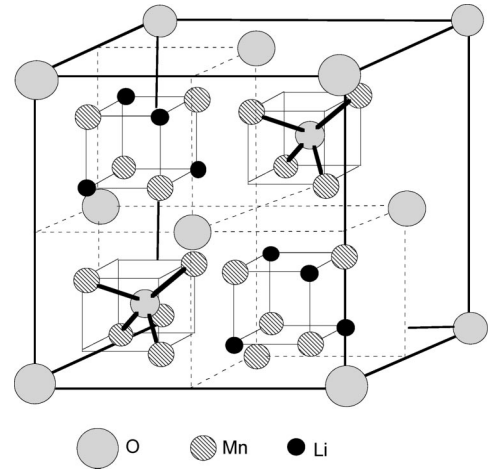

Figure 1. Spinel lattice of the sample. The lattice sites are distinguished by the color: gray, oxygen; dashed, Mn (octahedral site); black, Li (tetrahedral site). The dashed cubes also occupy the back-half of the unit cell. Note the cations (Mn) occupy only 1/2 of the octahedral sites.

* To whom correspondence should be addressed. E-mail: alain.mauger@impmc.jussieu.fr.

(1) Thackeray, M. M.; David, W. I. F.; Bruce, P. G.; Goodenough, J. B. *Mater. Res. Bull.* **1983**, *18*, 461.
(2) Thackeray, M. M.; Johnson, P. J.; de Picciotto, L. A.; Bruce, P. G.; Goodenough, J. *Mater. Res. Bull.* **1984**, *19*, 461.

10.1021/cm900609n CCC: $40.75
Published on Web 05/01/2009

ing the substitution concentration y, the oxidation state of manganese increases to maintain charge neutrality, up to the end member (Li)$[Li_{1/3}Mn_{5/3}]O_4$ (or $Li_4Mn_5O_{12}$) where all the manganese ions are in the Mn^{4+} valence state. The $[Mn^{IV}]O_6$ framework of (Li)$[Li_{1/3}Mn_{5/3}]O_4$ spinel is an attractive host structure for lithium insertion-extraction reaction. The reason is that only half of the octahedral sites are occupied by the cations in the ideal structure (see Figure 1), and it is then possible to insert Li^+ ions on the vacant octahedral sites of $Li_4Mn_5O_{12}$ and form $Li_{4+x}Mn_5O_{12}$.

Since all the manganese ions are in the Mn^{4+} valence state in $Li_4Mn_5O_{12}$, the lattice is expected to be less fragile than $LiMn_2O_4$ that is poisoned by many impurity phases, depending on the mode of preparation. Still, $Li_{1+y}Mn_{2-y}O_4$ prepared from the reactive system MnO/Li_2CO_3 leads to different impurity phases including Mn_3O_4, stroichiometric $LiMn_2O_4$ in addition to the nonstochiometric $Li_{1+y}Mn_{2-y}O_4$, and Li_2MnO_3 impurity phases.[4,5] Wet chemistry is the synthesis process that is so far most powerful to get rid of them, the reason why we have chosen this route in the present work.[6] Actually, only the Li_2MnO_3 impurity remains in this case. However, the amount of this impurity increases with the composition parameter y.

In our prior work,[6] attention has been focused on the characterization of $Li_{1+y}Mn_{2-y}O_4$ by magnetic measurements and optical experiments. We use these techniques here to determine the concentration of Li_2MnO_3 impurity in the solid solution of initial composition $Li_{1.33}Mn_{1.67}O_4$ spinel obtained by the sol−gel method. Moreover, we find that the presence of this impurity phase disproportionate to give Li_2MnO_3 impurity according to reaction:[7]

$$Li_{1+y}Mn_{2-y}O_4 \leftrightarrow (1 - z)Li_{1+y'}Mn_{2-y'}O_4 + zLi_2MnO_3 + \frac{z}{2}O_2 \quad (1)$$

where $y' = (y - z)/(1 - z)$ is the final composition of the spinel part of the final product. The structural analysis reported in the present work shows that $y' = 0.27$, against $y = 0.33$. This is in agreement with results obtained, for example, in ref 7, according to which eq 1 holds true for $y \geq 0.25$. The main effect of eq 1, however, is not the amount z of the impurity phase, as was thought in the past, but the deviation of the composition y' of the spinel part from the stoichiometric value $y = 1/3$, implying a noninteger value of the valence of the manganese ions. In materials that are far from a correlation-driven insulator−metal transition, the insulating character is preserved, and a noninteger value of the valence only results in a fraction of manganese in the Mn^{4+} valence state, the other part in the Mn^{3+} state, like in the case of $LiMn_2O_4$ for instance. Only two spinel-type oxides are known to be metallic, LiV_2O_4 that belongs to heavy-fermion compounds,[8] and $LiTi_2O_4$ that is a BCS superconductor.[9] Physical properties reported in this work suggest that $Li_{1+y'}Mn_{2-y'}O_4$ ($y' = 0.27$) also belongs to the heavy-fermion family. In particular, the magnetic properties are different from the ones expected from localized spins; The ESR spectra show a dysonian profile characteristic of metals; the specific heat varies linearly with temperature at low temperature, further evidence of the metallic behavior. In addition, the Sommerfeld constant is 2 orders of magnitude larger than the typical value in metals that are not highly correlated transition metal compounds. This outstanding property is linked to the fact that the magnetic interactions are fully frustrated by the combination of the geometric frustration of the spinel lattice, and the dilution of the $Mn^{3+}-O-Mn^{3+}$ interactions, so that no magnetic ordering is observed down to the lowest temperature (4.2 K) available in our experiments.

The electrochemical properties show that, at a 1C rate, the capacity of $Li_{1+y'}Mn_{2-y'}O_4$ ($y' = 0.27$) is as large as 163 mA h/g, because the material can be discharged up to $Li_{2.27}Mn_{1.73}O_4$, where the average valence of Mn is 3.3 only. This tolerance upon discharge below the average valence of 3.5 may also be the consequence of the metallic character that screens the Coulomb interaction and prevents the Jahn−Teller distortion associated with the presence of Mn^{3+} ions when the ionic description holds true, i.e., in the insulating phase.

2. Experimental Section

Powder of nominal composition $Li_{1.33}Mn_{1.67}O_4$ was prepared by the wet chemistry technique described in ref 10. The aqueous solutions of lithium and manganese acetates were added to aqueous solution of succinic acid (chelating agent) and the mixture was heated. The carboxylic groups in the succinic acid form chemical bonds with the metal ions and the extremely viscous pastelike substance develops upon slow evaporation of water. The paste was dried at 110 °C to obtain the dry precursor. The precursor was then decomposed in air at around 400 °C and heat-treated for 6 h at 750 °C to complete synthesis of lithium manganese spinel.

The potentiometric-redox titration method was used to determine the total amount of manganese and its average oxidation state (AOS) in studied sample. The applied procedure was based on that described elsewhere.[11] In the first step, the sample dissolved in HCl was potentiometrically titrated with standard solution of $KMnO_4$ to obtain the total amount of Mn. In the second step, the sample dissolved in $FeSO_4$ solution (in nitrogen atmosphere) was titrated with potassium permanganate solution to determine the amount of manganese with oxidation state larger than 2. A small amount of phosphoric acid was added before titration to facilitate determination of the end point.

The phase purity and crystal structure of the sample were characterized by the X-ray powder diffraction (XRD) profile measured with Cu Kα radiation using a Philips X'Pert diffractometer equipped with a nickel monochromator. The XRD data were

(3) Gummow, R. J.; de Kock, A.; Thackeray, M. M. *Solid State Ionics* **1994**, *69*, 59.
(4) Massarotti, V.; Bini, M.; Capsoni, D. *Z. Naturforsch., A* **1996**, *51*, 267.
(5) Massarotti, V.; Capsoni, D.; Bini, M.; Azzoni, C. B.; Paleari, A. *J. Solid State Chem.* **1997**, *128*, 80.
(6) Kopec, M.; Dygas, J. R.; Krok, F.; Mauger, A.; Gendron, F.; Julien, C. M. *J. Phys. Chem. Solids* **2008**, *69*, 955.
(7) Choi, S.; Manthiram, A. *J. Electrochem. Soc.* **2000**, *147*, 1623.
(8) Kondo, S.; Johnson, D. C.; Svenson, C. A.; Borsa1, F.; Mahajan, A. V.; Miller, L. L.; Gu, T.; Goldman, A. I.; Maple, M. B.; Gajewski, D. A.; Freeman, E. J.; Dilley, N. R.; Dickey, R. P.; Merrin, J.; Kojima, K.; Luke, G. M.; Uemura, Y. J.; Chmaissem, O.; Jorgensen, J. D. *Phys. Rev. Lett.* **1997**, *78*, 3729.
(9) Johnston, D. C. *J. Low Temp. Phys.* **1976**, *25*, 145.
(10) Prabaharan, S. R. S.; Michael, S. S.; Julien, C. *J. Inorg. Mater.* **1999**, *1*, 21.
(11) Chen, J.-F.; Xia, Y.-X.; Choppin, G. R. *Anal. Chem.* **1996**, *68*, 3973.

collected for 40 s at each 0.0167° step over a 2Θ range from 10 to 80°. The GSAS was used for the Rietveld analysis.

Raman scattering spectrum has been measured in the spectral range 200−800 cm^{-1} at room temperature in a quasi-backscattering geometry. A Jobin-Yvon (model U1000) double monochromator with holographic gratings and a computer-controlled photon-counting system was used. The laser light source was the 514.5 nm line radiation from a Spectra-Physics 2020 argon-ion laser. To have a large signal-to-noise ratio, 12 successive scans recorded at a spectral resolution of 2 cm^{-1} were averaged.

The magnetic properties have been investigated in the temperature range 4−300 K. Both the isothermal magnetization curves $M(H)$ in the field range 0−30 kOe and magnetic susceptibility at magnetic field 10 kOe (zero-field-cooled mode) were recorded using a SQUID (Superconducting Quantum Interference Device) magnetometer equipped with a liquid-helium-cooled amplifier to measure the magnetic moment in the range from 1×10^{-7} to 300 emu.

Electron spin resonance (ESR) measurements were performed at X-band frequency about 9.25 GHz using a Varian ESR spectrometer with TE102 rectangular microwave cavity. An ESR9 Oxford Instruments continuous flow cryostat allowed stabilization of temperature from 3.5 to 300 K. Powder samples were placed in a quartz tube purged with helium gas. Measurements were carried out during a heating run. The analysis of ESR derivative spectra recorded at magnetic field between 0 and 1 T was made by nonlinear least-squares fitting of multiple line shapes (Dysonian and Lorentzian). In addition, the Li_2MnO_3 sample was measured and the spectra were deconvoluted.

Specific heat was measured from 205 K down to 2 K using a thermal relaxation method employed by Quantum Design physical property system (PPMS).

The electrochemical properties of our sample (nominal composition $Li_{1.33}Mn_{1.67}O_4$) powder were measured at 25 °C in a cell with metallic lithium as negative electrode. Charge−discharge profiles were obtained at a 1*C* rate.

3. Results

3.1. Structural Properties. The average oxidation state of manganese determined experimentally by potentiometric-redox titration is 3.90 ± 0.06. Smaller than nominal (4.0) value of AOS is directly associated with the presence of additional phase Li_2MnO_3. The effective parameter y' in cubic $Li_{1+y'}Mn_{2-y'}O_4$ is smaller than the nominal parameter y; therefore, the average oxidation state is also smaller. It means that Mn^{3+} ions are present in the final product, whereas only Mn^{4+} ions are nominally expected in $Li_{1.33}Mn_{1.67}O_4$.

The X-ray diffraction (XRD) pattern of studied sample is presented in Figure 2. According to the Rietveld refinement, the sample prepared to be $Li_{1.33}Mn_{1.67}O_4$ is the mixture of two crystalline phases: Li_2MnO_3 (*C*/2*m*) and $Li_{1+y'}Mn_{2-y'}O_4$ in agreement with eq 1 with $z = 0.08$, and $y' = 0.27$ instead of the composition $y = 0.33$ that was initially expected (Rietveld parameters $R_{wp} = 0.011$, $R_p = 0.009$). With this value of y', the average valence of Mn in $Li_{1+y'}Mn_{2-y'}O_4$ is 3.89 instead of 4.0. This is in quantitative agreement with the value of y' deduced from titration measurements mentioned in the previous section, which gives evidence of the validity of eq 1, and is the confirmation that the composition of the cubic-spinel part of the final product is different from the nominal one.

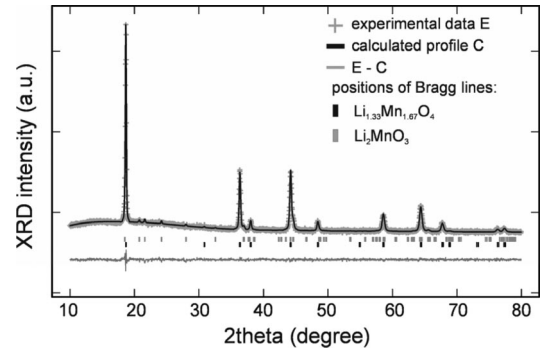

Figure 2. Output from the Rietveld refinement analysis of the XRD pattern for $Li_{1.33}Mn_{1.67}O_4$ sample. The + signs show experimental data, and the continuous line overlapping them refers to the calculated data. The vertical bars are the expected Bragg reflection positions. The difference between the experimental data and the calculated data is shown at the bottom. The *R* factors are $R_{wp} = 0.011$ and $R_p = 0.009$.

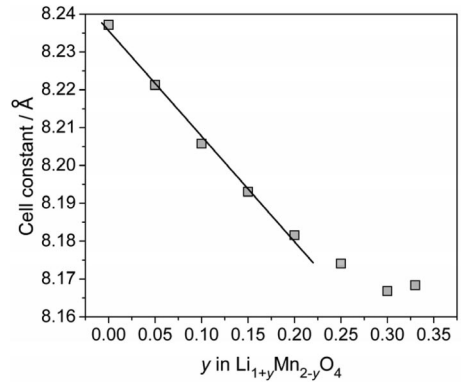

Figure 3. Lattice parameter as a function of the initial composition y of $Li_{1+y}Mn_{2-y}O_4$. The line is the linear law in the composition range where the disproportionation reaction is negligible.

After the scanning microscope image of this sample that has been reported elsewhere,[12] the average size of the powder particles is 70 nm, which compares well with the coherence length 50 nm of the lattice, deduced from the width of the XRD lines by application of the Scherrer's law.

Equation 1 also means that we have to reconsider the analysis of the physical properties that did not take this effect into account. Let us begin with the variations of the cubic lattice parameter a of $Li_{1+y}Mn_{2-y}O_4$ samples as a function of the composition we have reported in a prior work[6] and reproduced here in Figure 3. We find a fails to be linear in y (nominal composition), which we interpreted as a deviation from the Vegard's law. In particular, large deviations from linearity occur for $y \geq 0.25$, which is also the range of composition where the amount of Li_2MnO_3 impurity phase becomes large enough to be detected by XRD. Now we can assume that the Vegard's law is satisfied and the variations are linear as a function of the composition, provided we choose for this parameter the final composition y' instead of the nominal one y. Indeed, the quasi-linear variation of $a(y \approx y')$ in the region $y < 0.25$, where the amount of Li_2MnO_3 impurity phase is small, supports this assumption. The extrapolation of this linear law $a(y')$ down to the value $a =$ 8.1684(17) Å determined by the Rietveld refinement of the

(12) Dygas, J. R.; Kopec, M.; Krok, F.; Gendron, F.; Mauger, A.; Julien, C. M. *Electrochem. Soc. Trans.* **2007**, *3*−*36*, 179.

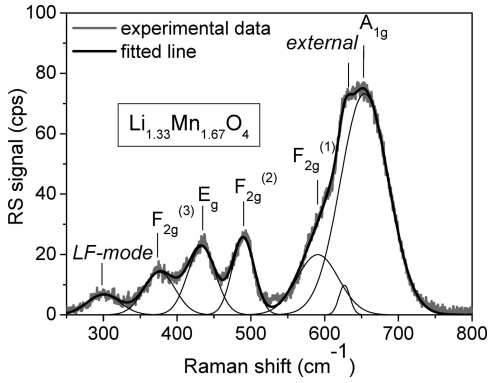

Figure 4. Raman spectrum of the sample of nominal composition $Li_{1.33}Mn_{1.67}O_4$. The thick solid lines correspond to the experimental data and fitted spectrum, the thin lines represent Gaussian line components of fitted spectrum. The LF (low-frequency) mode is related to Li vibrations. The external mode is associated with the $Mn^{4+}-O$ stretching mode in the Li_2MnO_3 impurity phase.

XRD spectra of the sample investigated here leads to the estimate $y' = 0.24$. This result is consistent with the value 0.27 determined from eq 1. This is the confirmation that the ansatz according to which the deviations of $a(y)$ from linearity are mainly due to the chemical process shown in eq 1, and the Vegard's law is indeed satisfied in the sense that $a(y')$ is linear. This linearity is also consistent with the fact that the cubic spinel phase is maintained without any deformation when lithium is introduced in the octahedral sites of the spinel, i.e., the lattice remains cubic, only the lattice parameter changes. As we shall see hereunder, eq 1 will also bring some enlightenment on magnetic properties.

The presence of Li_2MnO_3 phase is also observed in Raman spectrum of our sample reported in Figure 4. Seven Raman bands are observed as a result of decomposition with Gaussian profiles. The low-frequency mode at about 300 cm^{-1}, labeled *LF*-mode, is an unexpected mode always observed in this material, which could be Raman active because of the cationic disorder that induced a breakdown of the translation symmetry.[13] This mode is tentatively related to the stretching mode of Li in octahedral coordination.[14] The five other modes correspond to the allowed Raman-active modes, which can be labeled by their symmetry under O_h^7 spectroscopic group according to the irreducible representation $A_{1g} \oplus E_g \oplus 3F_{2g}$. The mode at the highest energy (630 cm^{-1}) is the external mode associated to the $Mn^{4+}-O$ stretching vibration of Li_2MnO_3 phase.[6] To investigate the validity of the assignment, we studied the *y*-dependence of the position and intensity of this mode. The results showed that the wavenumber of this mode shifts from 615 to 630 cm^{-1}, as the initial composition *y* increases from 0.15 to 0.33, whereas the strongest mode in Raman spectrum of Li_2MnO_3 sample (A_{1g}) is localized at about 612 cm^{-1}.[5] Moreover, the intensity of investigated mode increases with *y*, which is consistent with the correlated increase in weight fraction of Li_2MnO_3 phase.[6] We then conclude that the mode at 630 cm^{-1} in our sample is connected with the presence of the additional Li_2MnO_3 phase. It is, however, difficult to quantify the fraction of Li_2MnO_3 from these experiments.

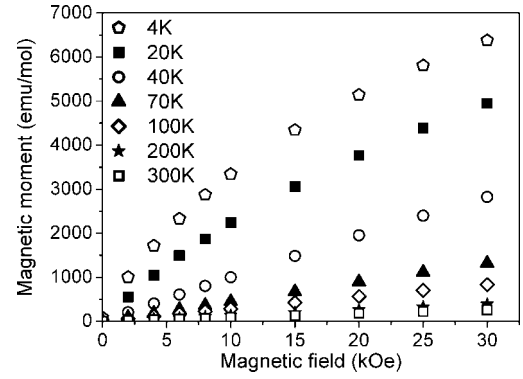

Figure 5. Magnetization curves $M(H)$ of the sample of nominal composition $Li_{1.33}Mn_{1.67}O_4$ recorded in the temperature range 4−300 K.

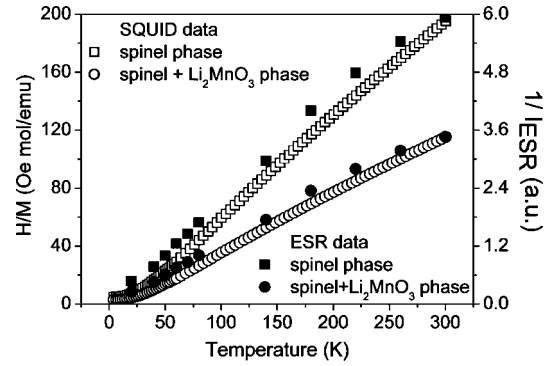

Figure 6. Temperature dependence of the inverse of the magnetic susceptibility measured under an applied field $H = 10$ kOe for the final product (nominal composition $Li_{1.33}Mn_{1.67}O_4$), before and after subtraction of the contribution of the impurity phase Li_2MnO_3. For comparison, the inverse of the integral intensity of the ESR spectra (Lorentzian plus Dysonian line, and Dysonian line alone) are also reported (full symbols).

3.2. Magnetic Properties. The magnetization curves $M(H)$ are reported in Figure 5. They are linear at $T > 80$ K. At lower temperature, however, a curvature is observed, due to the geometric frustration of the Mn magnetic moments on the B-sites and the dilution of the antiferromagnetic interactions, when *y* and *y'* increase.[6] The temperature dependence of the magnetization is presented in Figure 6 under the form of $H/M(T)$ measured at $H = 10$ kOe. In the temperature range 80−300 K, $H/M(T)$ is the inverse of the magnetic susceptibility, $\chi^{-1}(T)$. At lower temperature, H/M depends on the magnetic field and this quantity is meaningless, but we shall analyze $H/M(T)$ only in the temperature range where it makes sense, which is also the temperature range where the Curie−Weiss law applies. However, the physical value of interest is not the magnetic susceptibility of one mole of the sample, $\chi(T)$, but the susceptibility of one mole of $Li_{1+y'}Mn_{2-y'}O_4$, χ_{spin}. According to eq 1

$$\chi_{spin}(T) = [\chi(T) - z\chi_{im}(T)]/(1 - z), \qquad (2)$$

where χ_{im} is the magnetic susceptibility of one mole of Li_2MnO_3. $\chi_{im}(T)$ has been measured on a Li_2MnO_3 sample that has been prepared for this purpose. Then $\chi_{spin}(T)$ has been determined from eq 2, with the values $y' = 0.27$, $z = 0.08$ appropriate to the sample. The result is reported in Figure 6 under the form $\chi_{spin}^{-1}(T)$. The Curie−Weiss law is satisfied in the temperature range $T > 80$ K, from which we can deduce the effective magnetic moment carried by the manganese moment in $Li_{1+y'}Mn_{2-y'}O_4$: $\mu_{eff} = 3.54\ \mu_B$. Let

(13) Julien, C. M.; Massot, M. *J. Phys.: Condens. Matter* **2003**, *15*, 3151.
(14) Julien, C.; Letranchant, C.; Lemal, M.; Ziokiewicz, S.; Castro-Garcia, S. *J. Mater. Sci.* **2002**, *37*, 2367.

us assume for the moment that the material is insulating so that the magnetism originates from the spins that can be considered as localized on manganese ions. For $y' = 0.27$, the average valence of Mn is 3.89, which corresponds to 89% of the manganese ions in the Mn^{4+} state, and 11% in the Mn^{3+} state. The effective magnetic moment is then

$$\mu_{\text{eff}}^2 = 0.89[\mu(Mn^{4+})]^2 + 0.11[\mu(Mn^{3+})]^2. \qquad (3)$$

The magnetic moments of Mn^{4+} and Mn^{3+} are $\mu(Mn^{4+}) = 3.87$ and $\mu(Mn^{3+}) = 4.90\ \mu_B$ in the high-spin state, so the theoretical value deduced from eq 3 is $\mu_{\text{eff}} = 4\ \mu_B$, much larger than the experimental value. We then recover the result that we already outlined in ref 6 according to which the experimental effective momentum of Mn^{4+} is anomalously small in this material. The main consequence is that this material is quite a unique case where the analysis of the magnetization is not suitable tool to determine quantitatively the amount of impurity phase, at contrast with the situation met in manganese ionic compounds also used as cathode elements,[15] including $LiMn_2O_4$.[6] Actually, The small value of the effective moment implies that Mn^{3+} is in the low-spin state: $\mu(Mn^{3+}) = 2.83\ \mu_B$. Inserting this value in eq 3 leads to the theoretical value $\mu_{\text{eff}} = 3.76\ \mu_B$, which is consistent with the experimental data. The excess of 0.22 μ_B, however, is beyond experimental uncertainty. As we shall see hereunder, the smaller-than-expected magnetic moment is also linked to an unexpected profile of the ESR lines.

The ESR spectra of the sample are very broad, asymmetric lines, illustrated in Figure 7. They are well-reproduced by a superposition of a very broad Dysonian and narrow Lorentzian line. The integral intensity of the Dysonian line increases with decreasing temperature (Figure 8); that of the Lorentzian line too, but the dependence on temperature is much smaller, so that the origins of these two lines are different. On the other hand, the ESR spectra of the Li_2MnO_3 sample shows only one single Lorentzian line with g-factor $\cong 2$ and line width $\cong 0.232$ kOe at room temperature. This is the same Lorentzian line (same width, same center of line corresponding to g-factor $= 2$) as the one found by deconvolution of the spectra of the sample of nominal composition $Li_4Mn_5O_{12}$. In addition, we find that the temperature dependence of both the intensity and position of the Lorentzian lines are the same in Li_2MnO_3 and in the sample of nominal composition $Li_4Mn_5O_{12}$ (see Figure 6). Therefore, this narrow line is due to the manganese ions in Li_2MnO_3 (Mn^{4+} ions), and it can be used to measure the Li_2MnO_3 content in the sample of nominal composition $Li_{1.33}Mn_{1.67}O_4$. From comparison of the intensities of this line in the ESR spectra in the two samples, we find that the amount of Li_2MnO_3 phase in the final product of the sample of nominal composition $Li_{1.33}Mn_{1.67}O_{12}$ is in quantitative agreement with the value of z deduced from the structural analysis and from the titration measurements.

The broad Dysonian line (with constant g-factor) is the signal associated to the spinel part of the final product in eq 1. This physical origin of the broad Dysonian ESR line can be drawn based on the relation between the integral intensity and the magnetic susceptibility. It is known that the signal

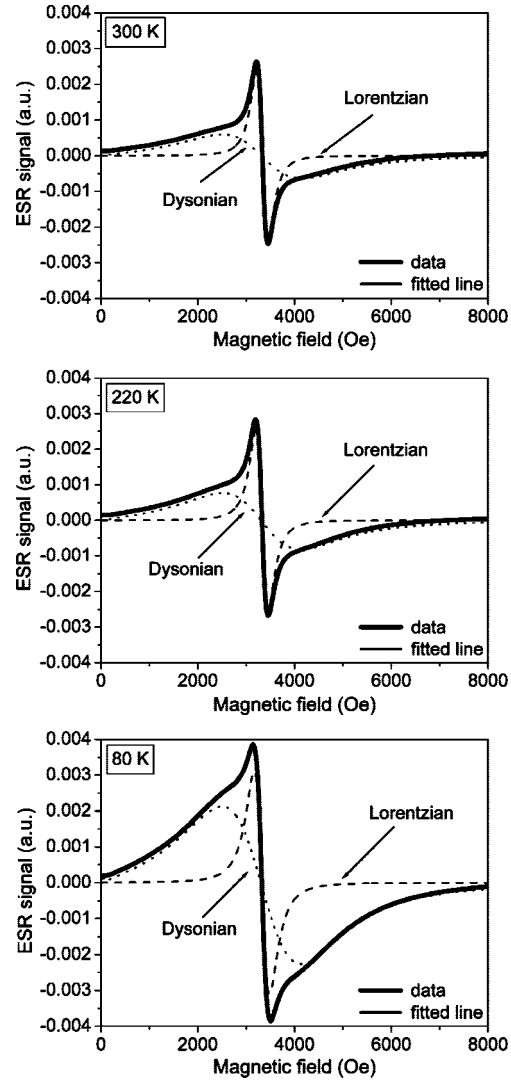

Figure 7. ESR spectra of $Li_{1.33}Mn_{1.67}O_4$ spinel measured at 300, 220, and 80 K. Solid lines correspond to the experimental data and fitted spectrum, dashed, and dotted lines are the Lorentzian and Dysonian line shape components of the fitted spectrum.

intensity is proportional to magnetic susceptibility. Indeed, we find that the temperature dependence of the integral intensities of the Dysonian broad line and the full ESR spectra (Dysonian plus Lorentzian lines) reproduce the susceptibility curves of the spinel part and of the final product, respectively. This is illustrated in Figure 6.

The fact that the signal associated to the spinel is of the Dysonian shape is in agreement with prior works,[5,12] but it is also a surprise, because this profile is typically ascribed to the magnetic resonance of electrons (or holes) in conducting materials when the electron concentration is large enough to produce the so-called spin-depth effect. In this case, the resonance of electrons is observed in a surface layer of thickness δ given by

$$\delta = \left(\frac{2c^2\varepsilon_0\rho}{\omega}\right)^{1/2} \qquad (4)$$

where ρ is the electrical resistivity and ω is the angular frequency of the radiation: $\omega/(2\pi) = 9.25$ GHz. The symmetric Lorentzian line shape gives way to the asymmetric dysonian line when δ becomes comparable to the thickness of the sample.[16]

(15) Kopec, M.; Yamada, A.; Kobayashi, G.; Nishimura, S.; Kanno, R.; Mauger, A.; Gendron, F.; Julien, C. M. *J. Power Sources* **2008**, doi: 10.1016/j.jpowsour.2008.12.096, in press.

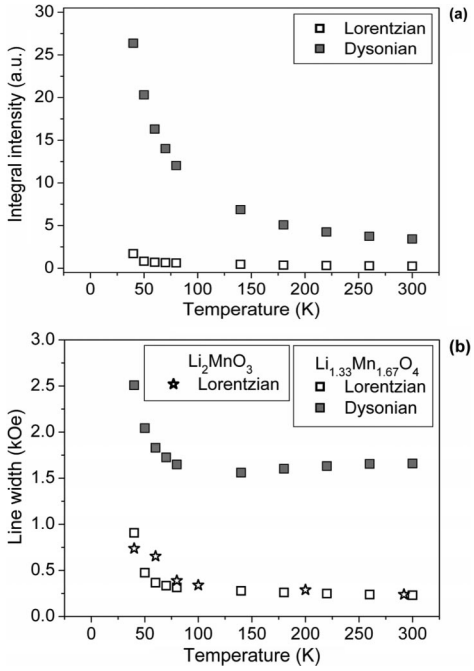

Figure 8. Temperature dependence of the (a) integral intensity and (b) the line width of the Dysonian and the Loentzian ESR lines for the sample of nominal composition $Li_{1.33}Mn_{1.67}O_4$.

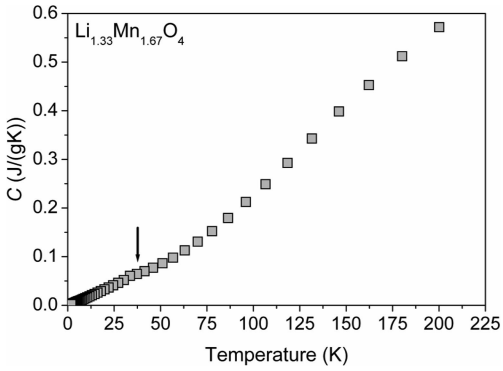

Figure 9. Specific heat of the sample of nominal composition $Li_{1.33}Mn_{1.67}O_4$. The arrow points to the Néel temperature of the impurity phase.

Transport experiments are always difficult interpret in thin powders, due to surface effects (we shall discuss them later on in this work). The metallic character is then better checked by heat capacity measurements that do not require any electric contact between the particles to probe the free electrons when they exist.

3.3. Specific Heat Measurements. The specific heat $C(T)$ of the sample is reported in Figure 9. At low temperature ($T < 60$ K), the specific heat is linear in temperature, which is another proof of the existence of free carriers. This is a major difference with $LiMn_2O_4$, for which $C(T)$ is reported in Figure 10 for comparison, for the two samples identified by the sintering temperature at 750 and 800 °C in ref 6. Indeed, this linear term is missing in this case, as expected since $LiMn_2O_4$ is not metallic. A significant positive curvature of the $C(T)$ curve can be detected only at $T > 60$ K, due to the T^3 contribution of the phonons. The Sommerfeld constant γ defined by $C(T) = \gamma T$ at low temperature is $\gamma =$

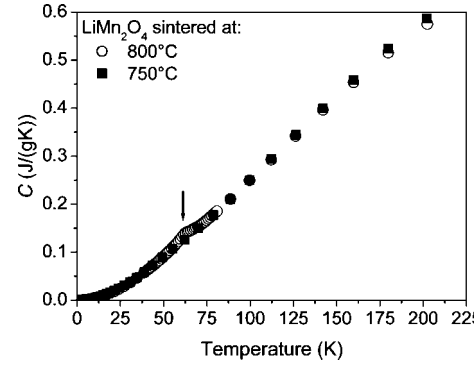

Figure 10. Specific heat of the two $LiMn_2O_4$ samples of ref 6 sintered at 750 and 800 °C. The arrow points to the Néel temperature, when it exists (see text).

308 mJ/K^2 mol (where mole refers to a mole of $Li_{1.27}Mn_{1.73}O_4$). This is comparable to the coefficient $\gamma =$ 420 mJ/K^2 mol met in LiV_2O_4,[8,17,18] characteristic of heavy fermion behavior.

In addition, the $C(T)$ curves show anomalies characteristics of the variation of the magnetic entropy associated to antiferromagnetic transitions. The secondary maximum at 36.5 K in the $C(T)$ curve of the sample of nominal composition $Li_{1.33}Mn_{1.67}O_4$ in Figure 9 is the signature of the antiferromagnetic ordering of the Li_2MnO_3 impurity phase at this temperature.[19] The secondary maximum of $C(T)$ in one of the $LiMn_2O_4$ in Figure 10 at 65 K corresponds to the Néel temperature of this compound.[20] On the other hand, no antiferromagnetic ordering could be detected in the $C(T)$ of the other sample of $LiMn_2O_4$ in Figure 10 because there is no long-range antiferromagnetic ordering in it. Indeed, the magnetic ordering in this material is rarely collective. Instead, a progressive formation of antiferromagnetic domains of finite size is observed, which can be only evidenced by neutron experiments that detect the coexistence of antiferromagnetic Bragg peaks with the magnetic diffuse peak in the range 65−10 K.[21]

3.4. Electrochemical Properties. The Li/$LiMn_2O_4$ cell discharges at 4 V. It corresponds to the extraction of lithium from 8*a* tetrahedral sites, the only sites occupied by the lithium in $LiMn_2O_4$. To the contrary, the Li/$Li_{1.27}Mn_{1.73}O_4$ cell exhibits no capacity in the 4 V region, which gives evidence that it is not possible to extract the lithium ions from the tetrahedral sites. The first discharge−charge profile of the Li/$Li_{1.27}Mn_{1.73}O_4$ cell (or equivalently Li/$Li_{3.8+x}Mn_{5.2}O_{12}$) is reported in Figure 11, in the voltage range 1.5 to 3.6 V. In this range, the initial cell has a capacity of 163 mA h/g (i.e., per gram of the spinel phase of the final product). This is in quantitative agreement with the theoretical capacity of composition $Li_{3.8+x}Mn_{5.2}O_{12}$ after the value of $y' = 0.27$, taking into account that the impurity phase is an inert mass in quantity given by $z = 0.08$ in eq 1 and taking into account that the spinel part can be discharged up

(16) Dyson, F. J. *Phys. Rev.* **1955**, *98*, 99.
(17) Johnson, D. C.; Swenson, C. A.; Kondo, S. *Phys. Rev. B* **1999**, *59*, 2627.
(18) Kondo, S.; Johnston, D. C.; Miller, L. L. *Phys. Rev.* **1999**, *59*, 2609.
(19) Strobel, P.; Lambert-Andron, B. *J. Solid State Chem.* **1988**, *75*, 90.
(20) Tomeno, I.; Kasuya, Y.; Tsunoda, T. *Phys. Rev. B* **2001**, *64*, 094422.
(21) Wills, A. S.; Raju, N. P.; Greedan, J. E. *Chem. Mater.* **1999**, *11*, 1510.

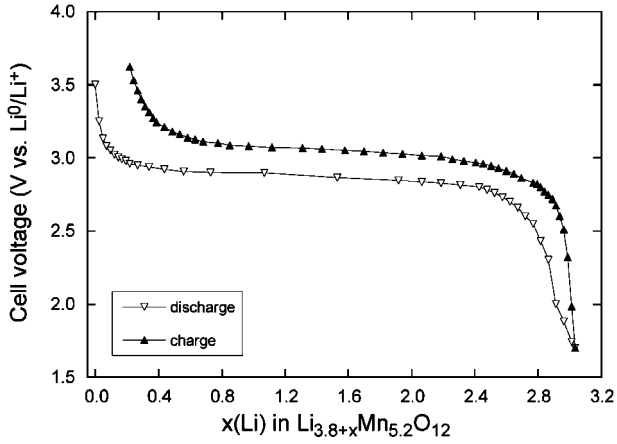

Figure 11. Discharge−charge profiles of cell Li//$Li_{1.27}Mn_{1.73}O_4$. Measurements carried out at the 1*C* rate show the characteristic plateau at 2.9 V vs Li^0/Li^+.

to the composition $x = 3.0$ after Figure 11. The plateau at 2.9 V is the Mn^{4+}/Mn^{3+} redox potential vs Li^0/Li^+ for Mn ions in the octahedral sites. The existence of this plateau is characteristic of a two-phase system, after the Gibbs phase rule, just like in the case of $Li/LiFePO_4$. Therefore, the electrochemical extraction/insertion of Li between $Li_{3.8}Mn_{5.2}O_{12}$ and $Li_{6.8}Mn_{5.2}O_{12}$ leads to the formation of the biphased system $uLi_{3.8+\alpha}Mn_{5.2}O_{12} + (1-u)Li_{6.8-\beta}Mn_{5.2}O_{12}$ ($0 \le u \le 1$). We still identify this material by the average composition $Li_{3.8+x}Mn_{5.2}O_{12}$ ($\alpha \le x \le 3-\beta$) for simplicity, but it should actually not be confused with the chemical formula of a solid solution. The homogeneous phase should exist only in the range $0 \le x \le \alpha$ and $x > 3-\beta$ where the voltage depends on x. Because the cell voltage reported in Figure 11 is measured at a 1*C* rate, we cannot take for granted that the cathode is at equilibrium, so that it is difficult to estimate the parameters α, β with a good accuracy, but typically $\alpha \approx 0.2$, $\beta \approx 0.5$. Note the average valence of Mn in the end member $Li_{6.8}Mn_{5.2}O_{12}$ is 3.3. This oxidation state of manganese cannot be achieved safely in $Li_{1+y}Mn_2O_4$ since in a static (cooperative) Jahn−Teller distortion of the lattice occurs very close to the stoichiometric composition ($y = 0.08$).[1] We thus find that the $Li_{1.27}Mn_{1.73}O_4$ cathode is more stable to overdischarge than $LiMn_2O_4$. Note this feature may be linked to the metallic character of the active material, because it avoids the Jahn−Teller distortion of Mn^{3+} in the insulating phased. The second advantage of the $Li_{6.8}Mn_{5.2}O_{12}$ cathode is an increased diffusivity of the lithium, because the lithium extracted from the octahedral sites has a binding energy reduced by 1 eV with respect to the Li^+ ions in the tetrahedral sites. This feature explains the performance of the cell at the relatively large rate of 1*C* in Figure 11. This reduction of the redox potential has a third advantage, namely, it avoids the instability of the organic-based electrolyte at high voltage reached when charging cells. The fourth advantage is the relatively high capacity. The capacity of 163 mA h/g is larger than the highest discharge capacity 118 mA h/g obtained at the same discharge rate of 1*C* in $LiMn_2O_4$,[22] and even larger than the capacity of 140 mA h/g delivered by $LiMn_2O_4$ at a lower rate.[23]

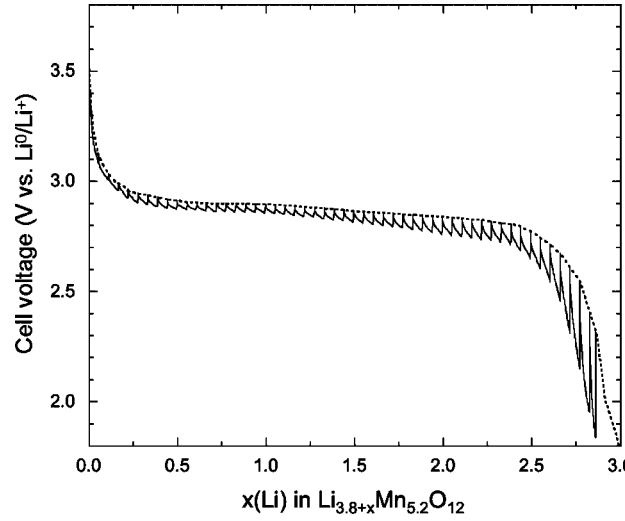

Figure 12. Discharge curve of cell Li//$Li_{1.27}Mn_{1.73}O_4$ with relaxation period showing the increasing IR drop upon Li insertion in the Li-rich side. Measurements were carried out in the galvanostatic mode with 52 steps of $\Delta x = 0.055$ each.

The evidence of the insulating phase on the Li-rich compound is illustrated in Figure 12. The galvanostatic discharge curve recorded with relaxation period between two Li injections into the $Li_{3.8}Mn_{5.2}O_{12}$ framework displays the increasing ohmic (IR) drop contribution, i.e. decreasing electronic conductivity of the active cathode material. Results indicate that the $Li_{3.8+x}Mn_{5.2}O_{12}$ insertion compound transforms toward the insulating regime for Li insertion $x > 2$. We shall see hereunder, in the discussion, the origin of this transition.

4. Discussion

The low value of μ_{eff} and the evidence for low-temperature metallic conductivity from the specific-heat data indicates that $Li_{3.8}Mn_{5.2}O_{12}$ contains low-spin Mn^{3+} ions with a localized majority-spin manifold $t^{3\uparrow}$ and minority-spin $t^{1\downarrow}$ electrons that are itinerant at low temperatures. The high-spin electrons are localized on the Mn atoms due to the strong intra-atomic exchange stabilization. The existence of the minority-spin electron, which has been proved by the low effective magnetic moment in this work, is thus crucial to explain the metallic behavior. In the same way, the spinel $Fe_3O_4 = Fe^{3+}[Fe^{3+}Fe^{2+}]O_4$, has majority-spin d^5 configurations and minority-spin t-electrons on the octahedral sites that are itinerant below room temperature.

The effective mass of the heavy-fermions can be derived from the Sommerfeld coefficient

$$\gamma = \frac{2}{3}\left(\frac{\pi k_B}{\hbar}\right)^2 m_0 (3\pi^2)^{-2/3} V\left(\frac{m}{m_0}\right) N^{-2/3} \qquad (5)$$

m_0 the mass of the free electron at rest, m the effective mass of the fermion, V is the volume. The volume V_0 of the unit cell is known from XRD experiments, so that the volume per $Li_{1.27}Mn_{1.73}O_4$ formula is $V_0/8 = 70$ Å^3. The fermions responsible for the metallic behavior are the $t^{1\downarrow}$ electrons

(22) Sengupta, S.; Roy, R. R.; McLean, A.; Dasgupta, S. *Can. J. Metal. Mater. Sci.* **2006**, *45*, 341.

(23) Yongyao, X.; Noguchi, H.; Yoshio, M. *J. Solid State Chem.* **1995**, *119*, 216.

issued from the Mn^{3+} ions; let us recall that there ae 11% of Mn^{3+} ions per $Li_{1.27}Mn_{1.73}O_4$ formula, so that $N = 0.11 \times 1.73 = 0.19$. m/m_0 is then readily deuced from eq 5, taking into account the experimental value of γ. The result is

$$m/m_0 = 467 \quad (6)$$

Heavy fermion behavior is found where the Fermi energy of an itinerant-electron band intersects the energy of a localized-electron redox couple. It has been first been observed in the family of lanthanides and uranides where the heavy fermion behavior is due to the *f*-electrons of the rare-earth element (the archetype of heavy-fermion systems is UPt_3). However, the 3d electrons of transition elements of the first series are also able to generate this behavior, although it is much less common. In spinel-oxides, the case of vanadium above-mentioned was quite unique prior the present work. However, we can also cite the case of iron in the skuterrudite $LaFePO_4$.[24]

The fact that the Curie−Weiss law is still satisfied, in the sense that χ^{-1} varies linearly with temperature is at first sight unexpected, because this law has been established in the framework of the theory of magnetism for localized spins. However, this behavior of the magnetic susceptibility is also observed in case the spin density is rather well localized in the vicinity of the transition element, whereas the charge density is delocalized. This situation is not uncommon. Examples are Mn- and Fe-based materials that crystallize in the NiAs structure,[25] and this situation is also met in Heusler alloys.[26] Yet in these examples, the metallic character did not give rise to heavy-fermion behavior, but we did met it in the $LaFePO_4$ heavy-fermion system.[24] In all these metals or semimetals, the only sizable difference with respect to the Curie law is the deviation of the Curie constant with respect to the theoretical value predicted in an ionic description, say the mixture of Fe^{2+} and Fe^{3+} in the case of skutterudites,[24,27] mixture of Mn^{3+} and Mn^{4+} in the present case. In particular, the orbital angular momentum is not quenched on the minority-spin electrons of $Li_{3.8}Mn_{5.2}O_{12}$. The deviation of the Curie constant that is lower than the value predicted from the ionic description of the material can then be considered as the first evidence of the metallic character of $Li_{1.27}Mn_{1.73}O_4$, confirmed by the specific heat measurements.

Another condition needed to have a heavy-fermion behavior is that the Coulomb interactions that favor the Fermi liquid behavior at low temperature overcome the magnetic interactions that favor the magnetic ordering. As a consequence, no magnetic ordering is observed. This is the case in LiV_2O_4, and in $LaFe_4Sb_{12}$ above cited, and this is indeed also the case in $Li_{1.27}Mn_{1.73}O_4$. The specific heat measurement is a very sensitive tool to determine the existence of a magnetic ordering, and actually much more sensitive than the magnetic susceptibility in case of antiferromagnetic interactions. In particular, the antiferromagnetic ordering of the Li_2MnO_3 impurity phase the sample of nominal composition $Li_{1.33}Mn_{1.67}O_4$ could be detected on the $C(T)$ curves in Figure 9, but not on the magnetic susceptibility curve $\chi(T)$ because the amount of impurity was too small. In the same way, the antiferromagnetic transition in $LiMn_2O_4$, when it exists, could be detected on the $C(T)$ curves in Figure 10, but not on the $\chi(T)$ curve of this sample.[6] The magnetic ordering could not be detected either on the $\chi(T)$ curve either in the FeSb compound crystallizing in the NiAs structure.[25] However, when it exists, the magnetic transition can be detected by specific measurements. Therefore, the lack of any anomaly of $C(T)$ of the sample of nominal composition $Li_{1.33}Mn_{0.67}O_4$ besides the Néel temperature of the impurity phase is the proof that there is no magnetic ordering in $Li_{1.27}Mn_{1.73}O_4$. Note also that the entanglement of the unquenched orbital momentum and spin of the minority-spin electrons can suppress long-range magnetic order. This situation has been found in $RTiO_3$ perovskites at $R \approx Gd$.[28]

This lack of ordering in this $Li_{1.27}Mn_{1.73}O_4$ spinel is in agreement with our previous work and the present data that show the effective Curie−Weiss temperature almost vanishes. In this material, like in other heavy-fermion systems, this lack of magnetic ordering is partly due to the geometric frustration of the antiferromagnetic interactions. This property inherent to the spinel lattice is even the main reason why LiV_2O_4 is a heavy-fermion system. However, in the present case, this is not sufficient, because $LiMn_2O_4$ can undergo an antiferromagnetic transition, as we have seen, and indeed, $LiMn_2O_4$ is not a heavy fermion system. It is even expected to be insulating at low temperature, in case the charge ordering associated with the Verwey transition becomes complete. Therefore, there is another source of the frustration of magnetic interactions that is responsible for the Coulomb correlation-driven insulator to metal transition in $Li_{1+y}Mn_{2-y'}O_4$ at some composition y'_c in the interval $0 < y'_c < 1/3$. This another source of frustration can be identified from our prior work as one approaches the insulator−metal transition from the insulating side,[6] because we have determined that the increase of *y'* results in the dilution of the $Mn^{3+}-Mn^{3+}$ interactions by decreasing the concentration of Mn^{3+} ions, whereas the $Mn^{4+}-Mn^{4+}$ interactions are negligible.

We have shown that the Dysonian profile in the ESR spectra takes its origin in the intrinsic properties of the spinel phase. The existence of a metallic impurity phase, which is at the origin of a dysonian line superposed to a Lorentzian line in the spectra of many semiconductors, is unlikely in the present case, because the integration of the ESR signal corresponds to the magnetization of the spinel phase, orders of magnitude too large to be attributable to a metallic impurity, and no impurity except Li_2MnO_3 (that is not conducting) has been observed in our sample.

The investigation of electrochemical properties have also revealed a metal to insulating transition as *x* increases in $Li_xMn_{5.2}O_{12}$ in the range $3.8 < x < 6.8$. We have already pointed out that only minority-spin d-electrons can generate

(24) Viennois, R.; Charar, S.; Ravot, D.; Haen, P.; Mauger, A.; Bentien, A.; Paschen, S.; Steglich, F. *Eur. Phys. J. B* **2005**, *46*, 257.
(25) Amornpitoksuk, P.; Ravot, D.; Mauger, A.; Tedenac, J. C. *Phys. Rev. B* **2008**, *77*, 144405.
(26) Kübler, J.; Williams, A. R.; Sommers, C. B. *Phys. Rev. B* **1983**, *28*, 1745.
(27) Viennois, R.; Ravot, D.; Tedenac, J. C.; Charar, S.; Mauger, A. *Mater. Sci. Eng., B* **2005**, *119*, 1.
(28) Zhou, H. D.; Goodenough, J. B. J. *Phys.C: Condens. Matter* **2005**, *17*, 7395.

a metallic behavior, and only the Mn^{3+} ions can have such an electron, provided they are in the low spin state. Therefore, the metal to insulator transition can also be viewed as a transition of Mn^{3+} ions from low- to high-spin state. That is why insertion of Li into $Li_{3.8}Mn_{5.2}O_{12}$ gives a broad two-phase region between it and insulating $Li_{6.8}Mn_{5.2}O_{12}$ (see figure 11); in the same way, $Li_{1-x}CoO_2$ undergoes a transition from low-spin Co to high-spin Co as Li is removed, which is also why the open circuit voltage of the battery with this cathode element is flat, for $0 < x < 0.5$.[29]

Instead of a metallic behavior, measurements of the electronic resistivity ρ shows that ρ is the order of 100 Ω.cm at room temperature, and follows approximately the Arrhenius law with an activation energy the order of 0.3 eV.[12] This lack of consistency between electronic conductivity and the other physical properties investigated in the present work suggest that the surface layer affects transport experiments, either because of a contact resistance, or because the surface layer is not metallic. The Li_2MnO_3 impurity phase can even play an important role, since it is insulating. This impurity is expected to be under the form of nanoparticles stuck at the surface of the $Li_{1.27}Mn_{1.73}O_4$ spinel particles. Even if 8% impurity phase is not sufficient to cover the whole surface of the spinel particles (the surface over volume ratio for particles of 70 nm in diameter is about 20%), the Li_2MnO_3 particles are placed between $Li_{1.27}Mn_{1.73}O_4$ spinel particles and thus alter the electronic conductivity. The importance of the surface layer on the physical properties is actually commonly met in systems that are, like in the present case, mesoscopic. For instance, the ESR signal of mesoporous silicon measured under the same conditions and same angular frequency as in the present work is a Lorentzian line because it is insulating, but it turns to a dysonian profile under the effect of the absorption of NH_3 as soon as the amount of NH_3 molecules absorbed corresponds to one monolayer, because of a transition of the whole silicon to a metallic phase.[30] We can also envision effects observed in insulators and semiconductors, which are brought by redox interactions between the solid and an absorbate. For instance, upon exposure to air, redox reaction in an adsorbed water layer at the surface of diamond provides the electron sink for the subsurface hole accumulation layer.[31] We have also found recently that exposure to air affects the surface layer of another cathode material, $LiFePO_4$,[32] and the physical properties, including the valence of iron, can be quite different in the surface layer from those of the bulk.[33,34] At least, we know that the surface layer in the present case is not metallic, otherwise the conductivity would not be activated like in C-$LiFePO_4$ for instance.[35,36] Further investigations of the electronic properties of $Li_{1.27}Mn_{1.73}O_4$ have to be made on bulk materials, or at least on particles big enough to minimize surface effects before any conclusion on the electronic conductivity of $Li_{1.27}Mn_{1.73}O_4$ can be made.

5. Conclusions

The disproportionation reaction of $Li_{1.33}Mn_{1.67}O_4$ modifies the composition and the properties of the final product, which have been investigated by different techniques. A self-consistent analysis of the XRD spectrum, chemical titration, and ESR spectroscopy show that the composition of the spinel-phase in the final product is $Li_{1.27}Mn_{1.73}O_4$. The counterpart is the Li_2MnO_3 impurity phase in quantity that could be determined by both XRD analysis and ESR spectroscopy, and found in agreement with the disproportionation reaction. As a consequence the average oxidation state of manganese is smaller than expected. The noninteger valence of Mn, combined with the frustration of the magnetic interaction is responsible to a correlation-driven transition to the heavy-fermion metallic state that is consistently evidenced by both the heat capacity measurement and the dysonian profile of the ESR line associated to the spinel part of the final product. These results also give enlightenment on the reason why $Li_4Mn_5O_{12}$ segregates out the phase $Li_{3.8}Mn_{5.2}O_{12}$. $Li_4Mn_5O_{12}$ is an insulator (no Mn^{3+} ions), but close to an insulator−metal transition. The transition to the metallic phase that is made possible by introduction of Mn^{3+} in the low-spin state stabilizes the structure and avoids the Jahn−Teller deformation. Insertion of Li into $Li_{3.8}Mn_{5.2}O_{12}$ gives a broad two-phase region between it and $Li_{6.8}Mn_{5.2}O_{12}$, because of a transition from metal to insulating phase, which is expected to be a transition of Mn^{3+} from low-spin to high-spin state upon lithiation. However, the electronic transport properties, which are most sensitive to surface effects, suggest that the surface layer is not conducting and has different properties that need further exploration. In particular, we are eager to have reports on transport properties on thick single crystals, like in the case of LiV_2O_4.[37]

CM900609N

(29) Hertz, J. T.; Huang, Q.; McQueen, T.; Klimczuk, T.; Bos, J. W. G.; Viciu, L.; Cava, R. *J. Phys. Rev.* **2008**, *B 77*, 075119.
(30) Chiesa, M.; Amato, G.; Boarino, L.; Garrone, E.; Geobaldo, F.; Giamello, E. *Angew. Chem., Int. Ed.* **2003**, *42*, 5032.
(31) Maier, F.; Riedel, M.; Mantel, B.; Ristein, J.; Ley, L. *Phys. Rev. Lett.* **2000**, *85*, 3472.
(32) Zaghib, K.; Dontigny, M.; Charest, P.; Labrecque, J. F.; Guerfi, A.; Kopec, M.; Mauger, A.; Gendron, F.; Julien, C. M. *J. Power Sources* **2008**, *185*, 698.
(33) Zaghib, K.; Mauger, A.; Gendron, F.; Julien, C. M. *Chem. Mater.* **2008**, *20*, 462.
(34) Zaghib, K.; Liang, G.; Labrecque, J.; Mauger, A.; Julien, C. M.; Gauthier, M. *PRIME Pacific Rim Meeting on Electrochemical and Solid-State Science*; Honolulu, HI, Oct 12−17, 2008, 2008; The Electrochemical Society and The Electrochemical Society of Japan: Pennington, NJ, and Tokyo, 2008; Extended Abstract #582.
(35) Zaghib, K.; Mauger, A.; Goodenough, J. B.; Gendron, F.; Julien, C. M. *Chem. Mater.* **2007**, *19*, 3740.
(36) Mauger, A.; Zaghib, K.; Gendron, F.; Julien, C. M. *Ionics* **2008**, *14*, 209.
(37) Urano, C.; Nohara, M.; Kondo, S.; Sakai, F.; Takagi, H.; Shiraki, T.; Okubo, T. *Phys. Rev. Lett.* **2000**, *85*, 1052.